Free-to-bound recombination in near stoichiometric Cu_2ZnSnS_4 single crystals

S. Levcenko,[1,2,*] V. E. Tezlevan,[2] E. Arushanov,[2] S. Schorr,[1] and T. Unold[1]
[1]*Helmholtz Zentrum Berlin für Materialien and Energie GmbH, Hahn-Meitner-Platz 1, D-14109 Berlin, Germany*
[2]*Institute of Applied Physics, Academy of Sciences of Moldova, Chisinau, MD-2028, Moldova*
(Received 24 February 2012; revised manuscript received 3 May 2012; published 18 July 2012)

Cu_2ZnSnS_4 single crystals prepared by the chemical vapor transport technique were investigated by x-ray diffraction, chemical microprobe analysis, and Raman and photoluminescence spectroscopies. Single-crystal x-ray measurements show that Cu_2ZnSnS_4 crystallizes in the kesterite structure with the space group $I\bar{4}$ and unit cell parameters a = 5.4174(2) and c = 10.7903(7) Å at 150 K. Photoluminescence measurements show one broad asymmetric band peaked at 1.29 eV at low temperature. Temperature and excitation intensity dependencies of the luminescence band indicate that the transition is due to a free-to-bound recombination with an activation energy of 140 meV. We attribute this activation energy to the intrinsic acceptor-type Cu_{Zn} antisite defect in close agreement with results from density-functional theory. It is shown that by a detailed analysis of the temperature dependence of the free-to-bound luminescence transition the majority carrier density can be deduced, which in our case is estimated at $p \approx 10^{16}$ cm^{-3}.

DOI: 10.1103/PhysRevB.86.045206 PACS number(s): 61.72.−y, 78.20.−e, 78.55.−m

I. INTRODUCTION

The quaternary compound Cu_2ZnSnS_4 (CZTS) has attracted much attention as an absorber material for thin-film solar cells[1–6] as well as for a possible application in thermoelectric[7,8] and photocatalytic water-splitting[9,10] devices. With regard to CZTS solar cell devices, considerable improvement in the conversion efficiency has been achieved with a current demonstrated value of 8.4%.[4] This value has been even exceeded for the related pentenary selenium-containing compound $Cu_2ZnSn(S,Se)_4$ (CZTSSe) with a record efficiency of 10.1%.[3] Further improvement of CZTSSe-based solar cells requires a better knowledge of the basic properties of the material itself as well as of physical parameters that have a major impact on characteristics of the solar cells.[1] On the theoretical side, recent first-principles calculations for CZTSSe provided information on band structure,[11–13] optical properties,[12] and intrinsic defects.[13,14] On the experimental side, so far a few studies investigating the optoelectronic properties of polycrystalline CZTS thin films have been carried out[15–19] and even much less data on photoluminescence (PL) and vibrational properties of CZTS bulk single crystals[20–22] are available in literature. In most studies about CZTS, single crystals in the literature either structural, PL, or vibrational properties are reported, but in none of these studies all of the measurements have been performed for the same samples. This makes it difficult, if not impossible, to correlate the structural and electronic properties of this relatively unexplored new material. Thus, in the present work, a study of the PL properties of a nearly stoichiometric CZTS single crystal was combined with structural characterization by x-ray diffraction (XRD), wavelength dispersive x-ray spectroscopy (WDX), and Raman scattering in order to allow unambiguous conclusions about the defect properties and radiative recombination in this material.

II. EXPERIMENTAL DETAILS AND STRUCTURAL ANALYSIS

The CZTS single crystals were grown by the chemical vapor transport technique in a closed system with 5 mg iodine/cm^3 as the transport agent. A stoichiometric mixture of Cu, Zn, Sn, S (3N) elements was used as the starting material. The charge zone was maintained at 850 °C, and the growth temperature was 800 °C. Single crystals formed a black blade shape up to 5 mm × 1.5 mm in area and 1 mm in thickness. The grown crystals exhibited *p*-type conductivity as determined by the sign of the thermopower.

The chemical composition of the CZTS sample was examined by wavelength dispersive WDX performed on a JEOL-JXA 8200 electron microprobe analysis system with an accuracy of ±1 at. %. To ensure a high level of accuracy, the outcome of 20 individual local point measurements of the composition parameters were averaged. In order to obtain reliable results from the WDX measurements, the system was calibrated using elemental standards. By means of WDX measurements, the ratio of Cu:Zn:Sn:S was found to be 2.04:0.95:1.01:3.99, which reflects a near stoichiometric composition corresponding to CZTS with a slight Cu excess and Zn deficiency.

Data for the single-crystal structure determination of the CTZS sample were collected on an Oxford Diffraction Xcalibur diffractometer, equipped with a charge-coupled device (CCD) area detector Sapphire S and a graphite monochromator using Mo-Kα radiation (λ = 0.71073 Å). Suitable crystals were attached to glass fibers using perfluoropolyalkylether oil (ABCR GmbH & Co.) and transferred to a goniostat where they were cooled to 150 K for data collection. The size of the investigated crystal was about 0.32 × 0.30 × 0.23 mm^3. During the measurement 2068 reflections were collected, and out of them 531 were independent. The software packages CrysAlis CCD were used for data collection and CrysAlis Pro for cell refinement and data reduction.[23] An analytical absorption correction and an extinction coefficient of 1.05(9) were applied. In total 19 parameters were used. The refinement method of a full-matrix least-squares resulted in a goodness-of-fit on F^2 = 1.462.

Raman measurements were carried out at room temperature using the back-scattering configuration on a DILOR LabRam Micro-Raman system with unpolarized signal detection. A

 ©2012 American Physical Society

diode laser (457.9 nm) was used for excitation. The first-order Raman spectrum of a silicon wafer was measured as a reference before and after every single Raman spectrum. The spectra were corrected with respect to a silicon peak position of 520.7 cm^{-1}. All samples were probed at several arbitrarily chosen spots on the (112) plane.

The PL spectra were excited using a circularly polarized laser diode emitting at 670 nm on a (112) surface plane of the CZTS crystal. The luminescence signals were analyzed by using a 1/4 m grating monochromator equipped with a thermoelectrically cooled linear InGaAs diode array. Temperature-dependent measurements in a temperature range from 30 to 300 K were performed by mounting the sample on the cold finger of a closed-cycle He-cryostat.

III. RESULTS AND DISCUSSIONS

A. XRD analysis

Quaternary $A_2^I B^{II} C^{IV} X_4^{VI}$ compounds (with A-Cu; B-Zn, Fe; C-Sn; X-S, Se) may crystallize in the kesterite-type or stannite-type structure.[24] Both of these crystal structures are closely related but are assigned to different space groups due to a different cation distribution. The stannite-type structure is consistent with the $I\bar{4}2m$ symmetry, with the divalent cation located at the origin (Wyckoff position 2a) and the monovalent cation at the Wyckoff position 4d $(0,\frac{1}{2},\frac{1}{4})$. In the kesterite structure (Fig. 1), half of the monovalent cations occupy the Wyckoff position 2a (0,0,0), with the divalent and the remaining monovalent cation ordered at 2d $(0,\frac{1}{2},\frac{3}{4})$ and 2c $(0,\frac{1}{2},\frac{1}{4})$, respectively, resulting in the space group $I\bar{4}$. The four-valent cation is located at the Wyckoff position 2b $(0,0,\frac{1}{2})$ in both structures. The anion lies on the (110) mirror plane at the Wyckoff position 8i (x,x,z) for stannite and 8g (x,y,z) for kesterite, respectively.

The single-crystal x-ray diffraction structure determination resulted in the tetragonal space group $I\bar{4}$ with the lattice parameters a = 5.4174(2) Å and c = 10.7903(7) Å. In Table I the determined atomic coordinates are represented. According to the determined space group and Wyckoff positions, it is concluded, that the CZTS single crystal adopts the kesterite-type structure as previously reported for $Cu_2(Zn,Fe)SnS_4$ single crystals.[25] From the detailed refinement analysis, the metal-sulfur bond lengths were determined to be $d_{Cu(1)\text{-}S}$ = 2.3280(9) Å, $d_{Cu(2)\text{-}S}$ = 2.3288(16) Å, $d_{Zn\text{-}S}$ = 2.3268(16) Å, and $d_{Sn\text{-}S}$ = 2.3880(13) Å, whereas the bond angles within the cation tetrahedra are Cu(1)-S-Cu(2) = 110.35(7)°, Cu(1)-S-Zn = 110.42(6)°, Cu(2)-S-Zn = 110.73(4)°, Sn-S-Zn = 108.35(6)°, Cu(1)-S-Sn = 108.63(4)° and Cu(2)-S-Sn = 108.28(6)°. The determined anisotropic displacement parameters $U^i j$ are presented in Table II.

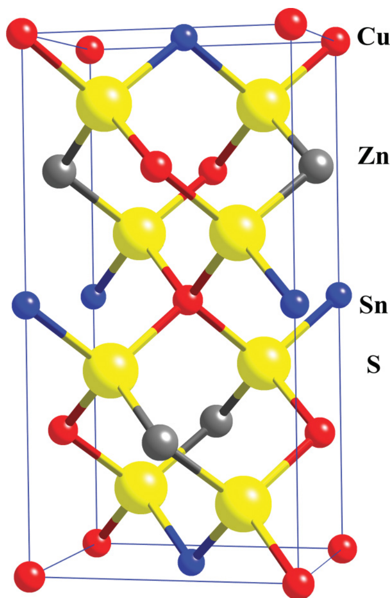

FIG. 1. (Color online) Unit cell representations of the kesterite-type structure.

TABLE I. Atomic coordinates and equivalent isotropic displacement parameters ($Å^2 \times 10^3$) for the CTZS single crystal. U(eq) is defined as one third of the trace of the orthogonalized U^{ij} tensor. The Wyckoff positions are in accordance to the space group $I\bar{4}$.

	x	y	z	Wyckoff site	U(eq)
Cu(1)	0.0	0.0	0.0	2a	12(1)
Cu(2)	0.0	0.5	0.25	2c	10(1)
Zn	0.0	0.5	0.75	2d	10(1)
Sn	0.0	0.0	0.5	2b	13(1)
S	0.2450(3)	0.2453(3)	0.1275(1)	8g	4(1)

B. Raman scattering

The kesterite structure ($I\bar{4}$ space group) of CZTS can be considered as a modification of the sphalerite structure in that the unit cell is derived by doubling the sphalerite cell in the $\boldsymbol{c}$ direction.[24] According to the unit cell group analysis of the irreducible representations for the zone center (Γ point), phonon modes are:[26,27] $\Gamma = 3A + 6B + 6E_1 + 6E_2$. All of these modes (a total of 21) are Raman active, whereas the species B, E_1, and E_2 are also IR active.

The Raman spectra of the CZTS single crystals are characterized by the presence of one characteristic intensive symmetric mode centered at 336 cm^{-1} and two additional less-pronounced modes around 286 and 371 cm^{-1} as shown in Fig. 2. These data are in agreement with Raman results previously reported in the literature on crystals (285, 336, and 362 cm^{-1}),[22] thin films (338 and 288, cm^{-1}),[18] and monograin powder (287, 338, and 368 cm^{-1}).[17] The dominant mode in the Raman spectrum at 336 cm^{-1} has been assigned to the

TABLE II. Anisotropic displacement parameters ($Å^2 \times 10^3$) for the CZTS single crystal. The anisotropic displacement factor exponent takes the form $-2\pi^2 [h^2a^2U^{11} + \cdots + 2 \cdot h \cdot k \cdot a \cdot b \cdot U^{12}]$.

	U^{11}	U^{22}	U^{33}	U^{23}	U^{13}	U^{12}
Cu(1)	13(1)	13(1)	11(1)	0	0	0
Cu(2)	10(1)	10(1)	9(7)	0	0	0
Zn	14(1)	14(1)	12(2)	0	0	0
Sn	10(1)	10(1)	8(1)	0	0	0
S	4(1)	4(1)	3(1)	0(1)	0(1)	0(1)

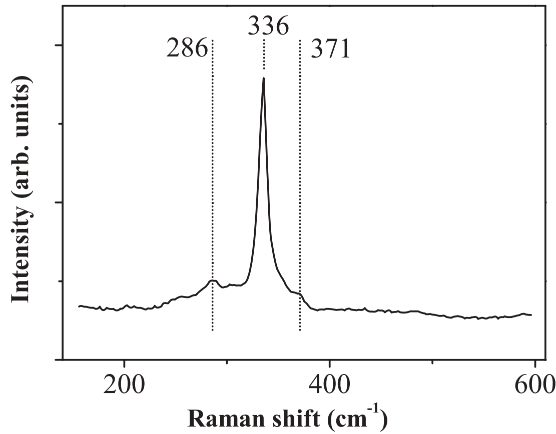

FIG. 2. Room-temperature Raman spectrum of the CZTS single crystal.

vibration of species A, which originates from the motions of the sulfur atoms alone in the kesterite lattice.[26]

In Fig. 2 the full width at half maximum (FWHM) of this mode is found to be 10 to 11 cm^{-1} for the studied CZTS crystals. This value is similar to the FWHM of 11–14 cm^{-1} for the 338 cm^{-1} mode recently reported on CZTS thin films[26,28] and indicates a significant amount of phonon localization due to lattice disorder in the thin films as well as in the single crystals.[29] The fact that the same FWHM was found at 100 K in Ref. 26 indicates a negligible thermal expansion contribution to the FWHM broadening. A possible reason for the phonon defect scattering processes is the cation disorder in the Cu + Zn layer of the kesterite structure caused by the small difference of 2.8 meV/atom between the kesterite and stannite phases of CZTS.[11,30]

According to the general findings for Raman spectra of $A_2^I B^{II} C^{IV} X_4^{VI}$ quaternary compounds,[22] the origin of the 286 cm^{-1} mode can be related to one of the symmetric A modes, described as a breathing mode of the SnS_4-tetrahedra. The assignment of the observed 371 cm^{-1} mode characteristic for CZTS[17,18,22] is less clear and may be related to vibrations of the E_1/E_2 and/or B mode due to its low intensity.[26] A more thorough identification of the observed modes will require polarization-dependent Raman and infrared studies of kesterite CZTS crystals and was beyond the scope of present study.

C. PL properties

Figure 3(a) shows the PL spectra of CZTS crystals measured with an excitation power of $P_{exc} \leqslant 1$ W/cm^2 at 30 K. The PL spectrum consists of one broad asymmetric band peaked around 1.29 eV, which is at considerably lower energy than the reported band gap of CZTS $E_g \approx 1.5$ eV,[6,21,31] and also much lower than the expected excitonic transitions for which the binding energy can be estimated at ≈40 meV, using the dielectric constant and effective mass from Ref. 12. A similar broad band centered at 1.2–1.3 eV was reported for single crystals,[20] thin films,[16] and monograin powders.[17] The peak position of the PL emission does not change noticeably with excitation intensity (P_{exc}) in the range from 10 to 740 mW/cm^2 as shown in Fig. 3(b), thus excluding a donor-acceptor pair transition for which a blueshift is

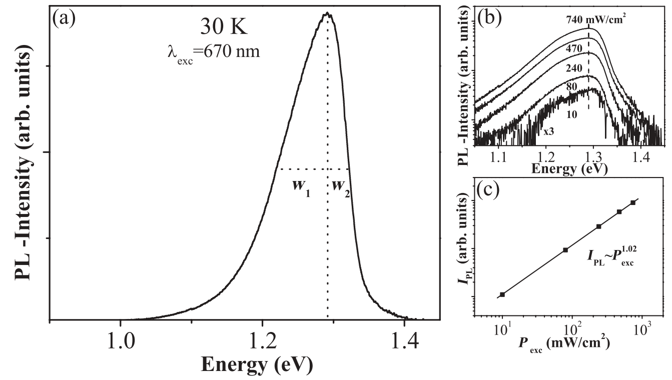

FIG. 3. PL spectra of the CZTS single crystal measured at 30 K and 740 mW/cm^2 (a). Dependence of the PL intensity (b) and integrated PL intensity (c) on excitation power at 30 K.

expected. In addition, it is found that the energy-integrated PL intensity (I_{PL}) depends linearly on the excitation intensity, $I_{PL} \sim P_{exc}$ [Fig. 3(c)]. Our results are in agreement with the excitation intensity-dependent PL results previously reported for a stoichiometric crystal[20] but are clearly distinct from the PL results reported for monograins powders,[17] sulphur poor crystals,[20] and thin films,[16] which all exhibit a large blueshift of the low-temperature PL-maximum of about 10–15 meV per decade.

The insensitivity of the peak position of the PL band on P_{exc} observed in the current study is typical for free-to-bound (FB) transitions. Since our crystals are of p-type conductivity, we assign the observed luminescence band to a conduction band-to-acceptor recombination. The asymmetric shape of the band and the absence of a large blueshift with increasing excitation intensity indicates that there is a distribution of acceptor states rather than a high compensation ratio, caused by high concentrations of both donor and acceptor-type defects.[17,19,32]

The evolution of the PL spectra and the half width at half maximum (HWHM) at the low (w_1) and high (w_2) energy side, respectively, with temperature rise from 30 to 300 K is shown in Fig. 4. It can be seen that the PL band shifts toward higher energy and that the asymmetry of the line

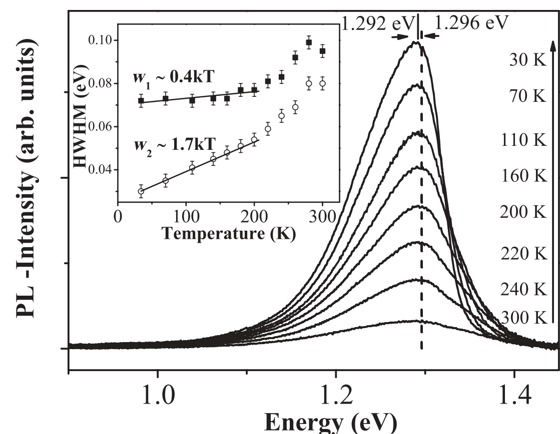

FIG. 4. Temperature dependence of PL spectra measured in the range of 30–300 K using an excitation power of 740 mW/cm^2 for CZTS single crystal. The inset shows temperature dependence of the HWHM parameters.

shape lessens. According to the theory of FB transitions between hydrogenlike impurity levels and the conduction or valence band,[33,34] a blueshift of the PL maximum and a linear law $0.45k_BT$ ($1.35k_BT$) for the HWHM at the low- (high-) energy side is expected with increasing temperature, where k_B is the Boltzmann constant. In our case the emission peak energy gradually increases from 1.292 to 1.296 eV in the range 30–100 K and saturates with a further increase of temperature. The calculated values of the temperature dependences of w_1 and w_2 are equal to $0.4k_BT$ and $1.7k_BT$ (inset on Fig. 4), respectively, in the range 30–200 K, which is in quite good agreement with the theoretical expectation. We relate the somewhat larger value observed for the temperature dependence of HWHM compared to the theoretical prediction to the observed broadening of the defect level.[32–34]

The variation of the I_{PL} with temperature is plotted in Fig. 5. It can be seen that at low temperatures, I_{PL} has a low rate of quenching, while above 190 K, it decreases very fast with increasing temperature. In the following we will analyze the temperature dependence of I_{PL} of free-to-bound transitions, in a way similar to the analysis of low-temperature PL suggested previously by Maeda[35] and Krustok *et al.*[36] The following processes were considered: (i) capture of a free hole by an acceptor level and (ii) recombination of a free electron with holes trapped at the acceptor level and (iii) thermal ionization of the trapped holes to the valence band. The following kinetic equation can be obtained

$$\frac{dN_A^-}{dt} = \Delta n\, \upsilon_{th}\sigma_n N_A^0 - p\upsilon_{th}\sigma_p N_A^- + \omega N_A^0 = 0 \qquad (1)$$

with

$$\omega = N_\upsilon \upsilon_{th}\sigma_p \exp(-E_{act}/k_BT)$$

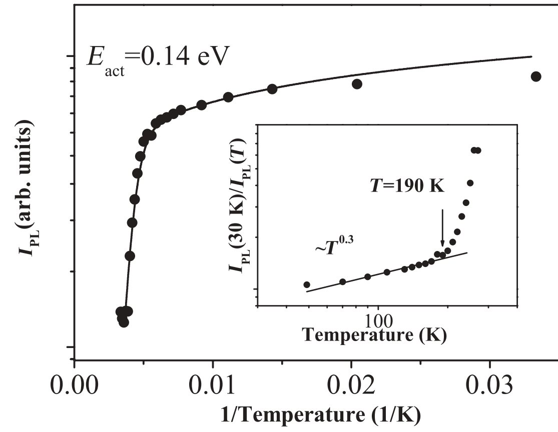

FIG. 5. Dependence of the integrated PL on temperature measured from 30 to 300 K using an excitation power of 740 mW/cm^2 for CZTS single crystal. The solid line shows the calculated result after Eq. (3). The inset shows the temperature dependence of the integrated PL plotted as $I_{PL}(30\ K)/I_{PL}(T)$ versus T.

where Δn resembles the excess carrier density of electrons proportional to the laser excitation and minority carrier lifetime, $N_A^0(N_A^-)$ represent an acceptor level filled (empty) with a hole, p is the hole concentration, σ_n/σ_p are the capture cross sections of a free electron/hole, υ_{th} is the thermal velocity, ω the thermal ionization probability of the trapped hole, N_υ the effective state density of the valence band, and E_{act} the energetic distance of the acceptor level with respect to the valence-band maximum. For these equations, low injection conditions, $\Delta p \ll p$ and $\Delta n > n$ are assumed. Taking into account that $N_A = N_A^- + N_A^0$, the temperature dependence of the FB emission intensity can be obtained from Eq. (1) as

$$I_{FB}(T) = \Delta n\upsilon_{th}\sigma_n N_A^0 = \frac{N_A}{1/\Delta n\upsilon_{th}\sigma_n + 1/p\upsilon_{th}\sigma_p + N_\upsilon \exp(-E_{act}/k_BT)/p\Delta n\upsilon_{th}\sigma_n}. \qquad (2)$$

To use Eq. (2), further simplifications have to be applied, since the exact temperature dependence of the carrier concentrations (Δn, p) and capture cross sections σ_p, σ_n are not independently known. With the assumption of $\Delta n \ll p$ (low injection conditions) and $\sigma_n/\sigma_p \leqslant 1$, we can neglect the second term in the denominator of Eq. (2). Using a power law approximation $\sim T^{-\alpha}$ for the temperature dependence of the product $\Delta n\upsilon_{th}\,\sigma_n$, Eq. (2) can be rewritten as

$$I_{FB}(T) = \frac{AT^{-\alpha}}{1 + \frac{N_\upsilon^*}{p}T^{3/2}\exp(-E_{act}/k_BT)}, \qquad (3)$$

where A is the constant, $N_\upsilon^* = 2(2\pi m_h k_B/h^2)^{3/2}$, m_h is the hole effective mass, and h is the Plank constant. The exponent α in Eq. (3) can be deduced from the low-temperature region, where the exponentional term of Eq. (3) can be neglected. The inset in Fig. 5 shows the integrated luminescence intensity, I_{PL}, of the CZTS crystal plotted as $\log(I_{30K}/I(T))$ from $\log(T)$. The data can be well described by a straight line with a slope of $\sim$0.3. Taking into account the temperature dependence of the thermal velocity $\upsilon_{th} \propto T^{1/2}$, this slope leads to a power law $\alpha \approx 0.8$ for the temperature dependence of $\Delta n\sigma_n$. Note that a distinction between the temperature dependencies of Δn and σ_n would require additional measurements such as time-resolved PL.

Assuming p to be independent of temperature in the fitting range, the best fit of Eq (3) to the experimental data in the whole temperature range was obtained for an activation energy $E_{act} = 0.14 \pm 0.02$ eV (see Fig. 5) with a preexponentional factor $N_\upsilon{}^*/p \sim 0.25$. From the prexponential factor, we can estimate the majority carrier density at room temperature $p \sim 10^{16}$ cm^{-3} when $N_\upsilon{}^*$ is calculated using a mean effective hole mass obtained from theory.[12] Note that this value for the majority carrier density estimated from the optical data is in good agreement with the typical values determined from capacitance voltage measurements[4,37] and Hall measurements[38] on CZTS.

The observed activation energy of 140 meV agrees well with the expected activation energy for a free-to-bound transition with a transition energy of $h\upsilon = 1.3$ eV and a band gap

of $E_g \approx 1.5$ eV,[6,21,31] considering the significant broadening of the defect transition. So far, there is no experimental report in the literature on a level with an ionization energy of 140 meV. Tanaka *et al.*[20] found an activation energy of 48 meV for a sulphur poor CZTS crystal, whereas no activation energy could be deduced for a stoichiometric crystal. Thin films have been found to exhibit PL quenching at low temperature with activation energies of 39(59) meV and 29–40 meV for stoichiometric (copper-poor) thin films[16] and copper-poor thin films with higher concentration of zinc,[19] respectively. For our CZTS crystal the composition was determined by microprobe to be slightly copper-rich and zinc-poor, suggesting Cu_{Zn} antisites as the dominant defect type. Indeed, first-principles calculations performed recently by Nagoya *et al.*[13] and Chen *et al.*[14] have suggested that the Cu_{Zn} antisites have the lowest formation energy and are the most stable defect in the entire stability range of CZTS and are thus the likely cause for the intrinsic *p*-type conductivity.[13] Furthermore structural studies by neutron diffraction indicated the presence of Cu_{Zn} antisites in near stoichiometric CZTS powder samples.[39] The calculated transition energy of 0.12 eV above the valence-band maximum for this Cu_{Zn} defect is in excellent agreement with the experimentally obtained activation energy of 140 meV observed in this study, given the uncertainties present in density-functional-theory-calculations and the significant broadening of the defect transition. We, therefore, conclude that the PL band observed for the CZTS crystal studied is due to a free-to-bound transition from the conduction band to a Cu_{Zn} antisite acceptor-type defect level.

Since this defect-related transition, rather than band-to-band or exciton-related transitions dominate the PL spectra, we conclude that, in order to optimize CZTS material for efficient solar cells, Cu_{Zn} antisites should be avoided by adjusting the growth processes accordingly, e.g., aiming at a sufficiently Cu-poor composition of the material.

IV. CONCLUSIONS

Near stochiometric CZTS single crystals were grown by the chemical vapor transport technique. Single-crystal XRD analysis confirmed that the crystals adopt the kesterite-type structure. Lattice vibration modes were observed at 286, 336, and 371 cm^{-1} in accordance with results in the literature for CZTS crystals and polycrystalline thin films. PL measurements showed a broad luminescence band centered at 1.29 eV, which from temperature and excitation intensity-dependent measurements is attributed to a free-to-bound transition with a thermal activation energy of 140 meV. With consideration of the slightly Cu-rich and Zn-poor composition of the single-crystal CZTS and recent predictions from density-functional theory, this transition is assigned to the Cu_{Zn} antisite acceptor-type defect, which has been predicted to have a low formation energy for a wide range growth conditions. We also derive an analytical description for the temperature dependence of the FB transition, which allows the estimation of the majority carrier density directly from the optical measurement.

ACKNOWLEDGMENTS

Financial support from STCU No. 5402 and IRSES PVICOKEST 269167 grants are acknowledged. The authors would like to acknowledge Elisabeth Irran (Technical University, Berlin) for her assistance during the single-crystal x-ray diffraction experiment and support in the data analysis. We thank Christiane Stephan for the chemical analyses of the samples.

*Corresponding author: sergiu.levcenco@helmholtz-berlin.de

[1] H. Katagiri, K. Jimbo, W. S. Maw, K. Oishi, M. Yamazaki, H. Araki, and A. Takeuchi, Thin Solid Films **517**, 2455 (2009).
[2] A. Redinger, D. M. Berg, P. J. Dale, and S. Siebentritt, J. Am. Chem. Soc. **133**, 3320 (2011).
[3] D. A. R. Barkhouse, O. Gunawan, T. Gokmen,T. K. Todorov, and D. B. Mitzi, Prog. Photovolt: Res. Appl. **20**, 6 (2012).
[4] B. Schin, O. Gunawan, Y. Zhu, N. A. Bojarczuk, S. J. Chey, and S. Guha, Prog. Photovolt: Res. Appl., doi: 10.1002/pip.1174 (2011).
[5] H. Katagiri, N. Sasaguchi, S. Hando, S. Hoshino, J. Ohashi, and T. Yokota, Sol. Energy Mater. Sol. Cells **49**, 407 (1997).
[6] B. A. Schubert, B. Marsen, S. Cinque, T. Unold, R. Klenk, S. Schorr, and H.-W. Schock, Prog. Photovolt: Res. Appl. **19**, 93 (2011).
[7] M. L. Liu, F. Q. Huang, L. D. Chen, and I. W. Chen, Appl. Phys. Lett. **94**, 202103 (2009).
[8] C. Sevik and T. Cagin, Phys. Rev. B **82**, 045202 (2010).
[9] S. Ikeda, T. Nakamura, T. Harada, and M. Matsumura, Phys. Chem. Chem. Phys. **12**, 13943 (2010).
[10] I. Tsuji, Y. Shimodaira, H. Kato, H. Kobayashi, and A. Kudo, Chem. Mater. **22**, 1402 (2010).
[11] S. Chen, X. G. Gong, A. Walsh, and S. H. Wei, Phys. Rev. B **79**, 165211 (2009).
[12] C. Persson, J. Appl. Phys. **107**, 053710 (2010).
[13] A. Nagoya, R. Asahi, R. Wahl, and G. Kresse, Phys. Rev. B **81**, 113202 (2010).
[14] S. Chen, J. H. Yang, X. G. Gong, A. Walsh, and S. H. Wei, Phys. Rev. B **81**, 245204 (2010).
[15] T. Tanaka, T. Nagatomo, D. Kawasaki, M. Nishio, Q. Guo, A. Wakahara, A. Yoshida, and H. Ogawa, J. Phys. Chem. Solids **66**, 1978 (2005).
[16] Y. Miyamoto, K. Tanaka, M. Oonuki, N. Moritake, and H. Uchiki, Jpn. J. Appl. Phys. **47**, 596 (2008).
[17] M. Altosaar, J. Raudoja, K. Timmo, M. Danilson, M. Grossberg, J. Krustok, and E. Mellikov, Phys. Status Solidi A **205**, 167 (2008).
[18] P. A. Fernandes, P. M. P. Salome, and A. F. Gunha, Thin Solid Films **517**, 2519 (2009).
[19] J. P. Leitao, N. M. Santos, P. A. Fernandes, P. M. P. Salome, A. F. daCunha, J. C. Gonzalez, G. M. Ribeiro, and F. M. Matinaga, Phys. Rev. B **84**, 024120 (2011).
[20] K. Tanaka, Y. Miyamoto, H. Uchiki, K. Nakazawa, and H. Araki, Phys. Status Solidi A **203**, 2891 (2006).
[21] K. Hönes, E. Zscherpel, J. Scragg, and S. Siebentritt, Physica B **404**, 4949 (2009).
[22] M. Himmrich and H. Haeuseler, Spectrochim. Acta, Part A **47**, 933 (1991).

[23]Oxford Diffraction (2008). CrysAlis CCD and CrysAlis RED Oxford Diffraction Ltd, Abingdon, Oxfordshire, England.
[24]W. Schafer and R. Nitsche, Mater. Res. Bull. **9**, 645 (1974).
[25]S. R. Hall, J. T. Szymanski, and J. M. Stewart, Can. Mineral. **16**, 131 (1978).
[26]P. K. Sarswat, M. L. Free, and A. Tiwari, Phys. Status Solidi B **248**, 2170 (2011).
[27]E. Kroumova, M. I. Aroyo, J. M. Pereyz-Mato, A. Kirov, C. Capillas, S. Ivantchev, and H. Wondratschek, Phase Transitions **76**, 155 (2003).
[28]H. Yoo and J. Kim, Sol. Energy Mater. Sol. Cells **95**, 239 (2011).
[29]C. Camus, E. Rudigier, D. Abou-Ras, N. A. Allsop, T. Unoldt, Y. Tomm, S. Scorr, S. E. Gledhill, T. Köher, J. Klaer, M. C. Lux-Steiner, and Ch. H. Fischer, Appl. Phys. Lett. **92**, 101922 (2008).
[30]S. Chen, A. Walsh, Y. Luo, J. H. Yang, X. G. Gong, and S. H. Wei, Phys. Rev. B **82**, 195203 (2010).
[31]S. Levcenco, D. Dumcenco, Y. P. Wang, Y. S. Huang, C. H. Ho, E. Arushanov, V. Tezlevan, and K. K. Tiong, Opt. Mater. **34**, 1362 (2012).
[32]A. P. Levanyuk and V. V. Osipov, Sov. Phys. Usp. **133**, 427 (1981).
[33]D. M. Eagles, J. Phys. Chem. Solids **16**, 76 (1960).
[34]A. Yamada, P. Fons, S. Niki, H. Shibata, A. Obara, Y. Makita, and H. Oyanagi, J. Appl. Phys. **81**, 2794 (1997).
[35]K. Maeda, J. Phys. Chem. Solids **26**, 595 (1965).
[36]J. Krustok, H. Collan, and K. Hjelt, J. Appl. Phys. **81**, 1442 (1997).
[37]K. Wang, O. Gunawan, T. Todorov, B. Schin, S. J. Chey, N. A. Bojarchiuk, D. Mitzi, and S. Guha, Appl. Phys. Lett. **97**, 143508 (2010).
[38]A. Nagaoka, K. Yoshino, H. Taniguchi, T. Taniyama, and H. Miyake, J. Cryst. Growth **341**, 38 (2012).
[39]S. Schorr, Sol. Energy Mater. Sol. Cells **95**, 1482 (2011).